ELSEVIER

Contents lists available at ScienceDirect

Journal of Magnetic Resonance

journal homepage: www.elsevier.com/locate/jmr



Pulsed spin-locking of spin-3/2 nuclei: ³⁹K-NQR of potassium chlorate

Kyle Edward Nixon, Karen L. Sauer*

George Mason University, 4400 University Drive, Fairfax, VA 22030, United States



ARTICLE INFO

Article history: Received 6 December 2021 Revised 3 January 2022 Accepted 10 January 2022 Available online 15 January 2022

Keywords:
Potassium chlorate
Spin-3/2
Powder sample
Quadrupolar nuclei
Half-integer quadrupoles
Nuclear quadrupole resonance
Pulse sequences
Zero-field NMR
Spin-lattice relaxation time
Spin-echo decay

ABSTRACT

A model was developed for predicting a locked signal under a series of refocusing pulses for Nuclear Quadrupole Resonance (NQR) of spin $I=\frac{3}{2}$ and tested with a powder of KClO₃. This work represents the first direct NQR detection of the 39 K line of potassium chlorate. The characteristic time constants, T_1, T_{2e} and T_2^* , were measured to determine the detectability of potassium chlorate via 39 K-NQR. The echo train T_{2e} was found to be strongly dependent on the refocusing pulse-spacing and weakly dependent on the refocusing pulse strength. The optimal angles of the excitation and echo pulse for a pulse train were also determined, as well as, the resonance-frequency dependence on sample temperature.

© 2022 Elsevier Inc. All rights reserved.

1. Introduction

Nuclear Quadrupole Resonance (NQR) is a phenomena arising from nuclei possessing spin greater than $\frac{1}{2}$ and utilizes radiofrequency pulses to excite a sample nucleus out of a ground state. Spin-3/2 is a prolific class of quadrupolar nuclei and as a result NQR techniques have numerous applications [1]. These applications range from thermometers [2–6] to investigating the internal orbital and magnetic order of materials, which is an important tool in the effort to create high T_c superconductors [7–9]. An important application for NQR is sample detection [10] as the nature of NQR allows one to determine the location and purity of a given sample. NQR has been the subject of study over the past several decades as a potential tool for the detection of nitrogen-based explosives [11,12].

Potassium chlorate is used in explosive devices, and is naturally of interest for NQR detection. The resonance frequencies of ³⁵Cl-NQR have been measured in KClO₃ [5,13] but are orders of magnitude higher than ¹⁴N-NQR [14]. System requirements for a device capable of detecting multiple different samples are greatly increased by a large disparity of target resonance frequencies. Furthermore, the large temperature dependency, 2.6 kHz/°C, of

E-mail addresses: knixon4@gmu.edu (K.E. Nixon), ksauer1@gmu.edu (K.L. Sauer).

chlorine NQR makes it attractive as a thermometer [5], but difficult to detect in uncontrolled environments. In contrast, as we confirmed, ³⁹K resonance frequency is close to other ¹⁴N lines of interest, such as ammonium nitrate, and possesses a temperature coefficient 4 times smaller than ³⁵Cl's. Previously, the ³⁹K line of potassium chlorate was not directly detected by NQR, but was indirectly detected through double-resonance [15].

NQR naturally generates a fairly weak signal, so optimizing the excitation sequence and its repetition is important. Therefore, we measured the relaxation rates key to efficient detection, including the decay of the spin-echoes as a function of pulse strength and timing. The spin-lock spin-echo sequence (SLSE) is one of the more common pulse sequences utilized to extend the signal in time. [16]. The sequence is composed of a single excitation pulse, which after a time of $\frac{1}{2}\tau$, is followed by a series of N refocusing pulses each separated by τ [17], $\Theta_x - \frac{\tau}{2} - \left[2\Theta_y' - \tau\right]^N$. The angle Θ is the nutation angle of the excitation pulse and $2\Theta'$ is the nutation angle of the echo pulse defined by

$$\Theta = \frac{\sqrt{3}}{2} \gamma B_1 t_1, \quad 2\Theta' = \frac{\sqrt{3}}{2} \gamma B_1' t_1' \tag{1}$$

where γ is the gyromagnetic ratio of ³⁹K, B_1 is the field strength of the pulse and t_1 is the duration of the pulse. The refocusing pulses have a phase shift of $\frac{\pi}{2}$ from the excitation pulse.

^{*} Corresponding author.

Previous work focused on predicting free induction decay and a single echo response in spin- $\frac{3}{2}$ NQR [18–20]. As shown in the Appendix A for many echoes, and decoherence dominated by electric field gradient inhomogeneity, the locked magnetic moment is at a minimum the same as for a single echo:

$$\bar{\mu}_{X-min} = S_0 \lambda \sin \lambda \Theta \sin^2 \lambda \Theta', \tag{2}$$

where S_0 is the magnetic moment from a single crystal and X is the axis of symmetry of the coil used both for excitation and detection. This magnetic moment, induced by an optimized single pulse, is defined as:

$$S_0 = \frac{\gamma \hbar^2 \omega \sqrt{3}}{4kT}, \tag{3}$$

where ω is the spacing between levels and T is the temperature of the sample. The excitation efficiency, λ , is given by [20]:

$$\lambda^{2} = \frac{\left[3(1 - \eta^{2}/3)\sin^{2}\theta + 2\eta\sin^{2}\theta\cos2\phi + \frac{3}{4}\eta^{2}\right]}{3 + \eta^{2}},$$
 (4)

The amplitude of the free induction is

$$\frac{S}{S_0} = \int_{\text{sphere}} \lambda \sin(\lambda \Theta) \frac{d\Omega}{4\pi},\tag{5}$$

where $d\Omega$ is the solid angle. In the limit $\eta = 0$,

$$\frac{S}{S_0} = \frac{\Theta}{3} + \frac{\pi H_1(\Theta)}{2\Theta} - \frac{\pi H_2(\Theta)}{2} \tag{6}$$

$$\approx \frac{4}{3} J_1(\Theta), \tag{7}$$

where H_n is the n^{th} order StruveH function. The last approximation uses the Jacobi-Anger expansion in terms of Bessel functions, retaining only the first order solution. Similarly, for the first echo and the locked signal, the signal is

$$\frac{S}{S_0} = \int_{sphere} \lambda \sin \lambda \Theta \sin^2 \lambda \Theta' \frac{d\Omega}{4\pi}.$$
 (8)

In the limit $\eta = 0$,

$$\begin{split} \frac{S}{S_0} &= \frac{\pi}{8\Theta\left(4\Theta'^2 - \Theta^2\right)} \times \left(-2\left(\Theta^2 - 4\Theta'^2\right)H_1(\Theta) + \Theta\left(\Theta + 2\Theta'\right)H_1(\Theta - 2\Theta') + \Theta\left(\Theta - 2\Theta'\right)\left[H_1(\Theta + 2\Theta') + \left(\Theta + 2\Theta'\right)\left\{2H_2(\Theta) - H_2(\Theta - 2\Theta') - H_2(\Theta + 2\Theta')\right\}\right]\right) (9) \\ &\approx \frac{2J_1(\Theta) - J_1\left(2\Theta' + \Theta\right) + J_1\left(2\Theta' - \Theta\right)}{3}. \end{split}$$

in which η is the asymmetry parameter, of the electric field gradient [1]; when the same coil is used both for excitation and detection, λ can also be viewed as the detection efficiency. The angles θ and ϕ correspond to $\widehat{X} = \sin\theta\cos\phi\widehat{x} + \sin\theta\cos\phi\widehat{y} + \cos\theta\widehat{z}$, the axis of symmetry of the excitation coil in the principal axis frame of the electric field gradient. Eqs. 2 to 4 give the result for a single crystal. In the next section these equations are used to predict the signal response of a powder sample from SLSE excitation.

2. Theory

2.1. Expected signal from a powder

Our derivation, detailed in Appendix A, closely follows the work of Goldman [20] and extends it to the case of spin-locking under N refocusing pulses with frequency ω_0 . Decoherence between pulses is assumed to be from a distribution of electric field gradients, and pulses are treated as delta-function. This assumption of inhomogenous broadening greatly simplifies the calculation, since the signal can be treated as the summation of off-resonant and resonant isochromats. Goldman's treatment of this system maps four dimensional spin space of spin-3/2 onto a Hilbert space of two spin-1/2.

Calculations for a powder sample are complicated by the excitation efficiency λ dependence on orientation shown in Eq. 4. However, as can be seen in Fig. 1, the mean of λ over a sphere does not vary appreciably with η , a conclusion shared with previous work [20,18]. Therefore we calculate the powder average in the limit that $\eta=0$, which is solvable analytically [20]. Moreover, other authors have shown the FID and echo response in a powder sample is insensitive to η , justifying the use of the $\eta=0$ limit [21,22,20], even though η is measured to be 0.69 in potassium chlorate through 39 K NMR [23].

Comparison between the exact and approximate solutions are given in Fig. 2. The approximate solution gives optimal values, both in pulse angles and signal size, within 5% of those for the exact solution. The maximum value, utilizing the approximations was calculated to return to 70 percent of the signal strength of a single crystal of comparable size and occurs at $\Theta=\Theta'=1.79$. Furthermore, one may note the deviation between the approximate solution, and the exact solution primarily exist within the higher Θ domains. The experimental data are fit to Eq. 10, for ease of calculation.

2.2. SNR

As shown in Appendix A.2, the signal-to-noise ratio (SNR) for NQR behavior is,

$$\label{eq:SNR} \textit{SNR} = \alpha \bigg\{ \frac{S_{\infty}}{2s} \, \sqrt{\frac{T_{2e}}{T_1}} \bigg\} \sqrt{T_{tot}},$$

where α is a factor, weakly dependent on the time constants, but of the order of unity, S_{∞} is the signal with infinite time between scans, s is the sensitivity of the sensor, and T_{tot} , is the total time taken to conduct all scans. Therefore measuring the echo-train decay, T_{2e} , and the spin-lattice relaxation decay, T_1 , is critical to determining the optimal SNR and ultimately the detectability of potassium chlorate.

3. Experimental set-up

In order to conduct the experiment, a probe designed for direct detection of potassium chlorate was constructed. The excitation coil, shown in Fig. 3, was part of a parallel-tuned tank circuit which used a capacitor in series to impedance match with the power amplifier. The probe was optimized for a frequency of 0.53 MHz,

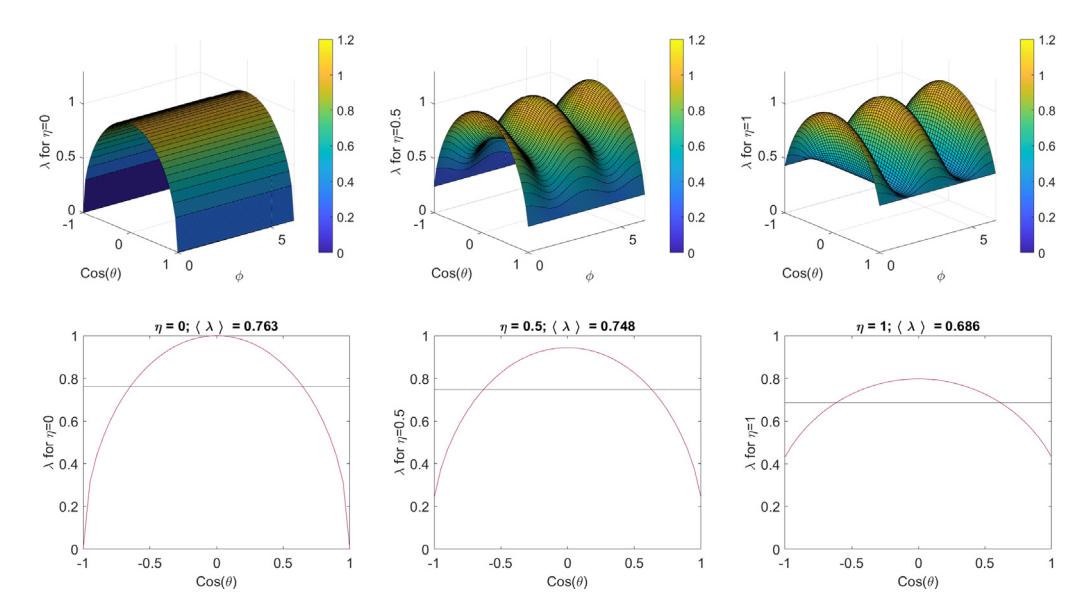


Fig. 1. Graph the excitation efficiency, λ , for a given value of η , the asymmetry parameter, over the domain of ϕ and $\cos\theta$, as described by Eq. 6.

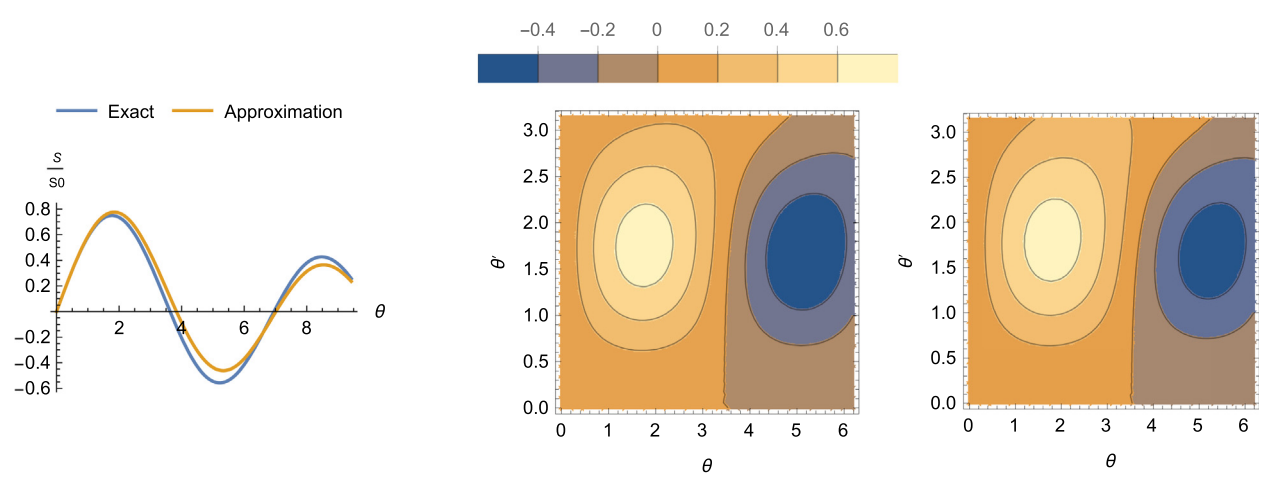


Fig. 2. Left: Expected signal, as a function of Θ , from a single excitation for both exact (blue) and approximate (yellow) solutions. Right: Expected echo/locked signal, as a function of Θ and Θ' , for both exact (center graph) and approximate (rightmost graph) solutions. Both exact and approximate solutions are taken in the limit $\eta = 0$.

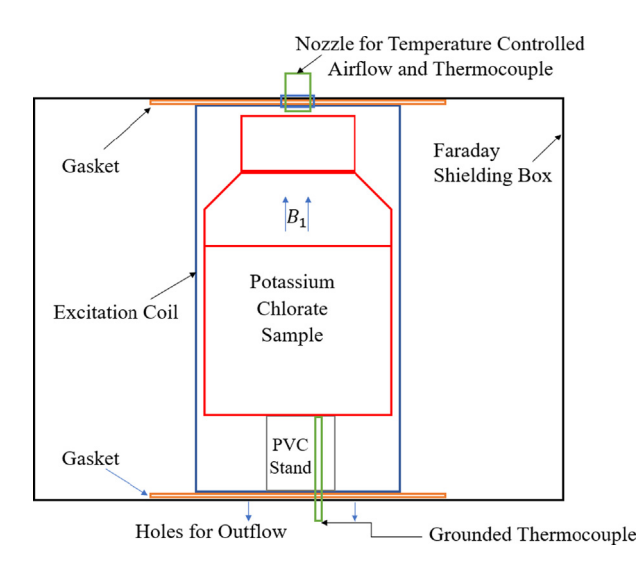


Fig. 3. The probe excited, and received signal from a temperature controlled [25] 1-kg powder sample of potassium chlorate.

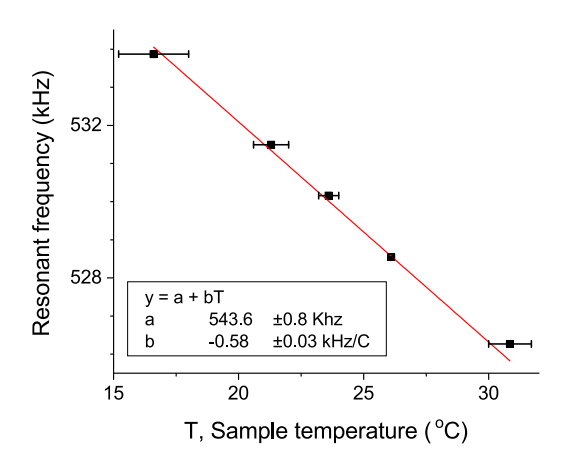


Fig. 4. The resonance frequency of $^{39}\rm K$ from potassium chlorate, KClO3, was found to vary at a rate of $-0.58~\rm kHz/^{\circ}C.$

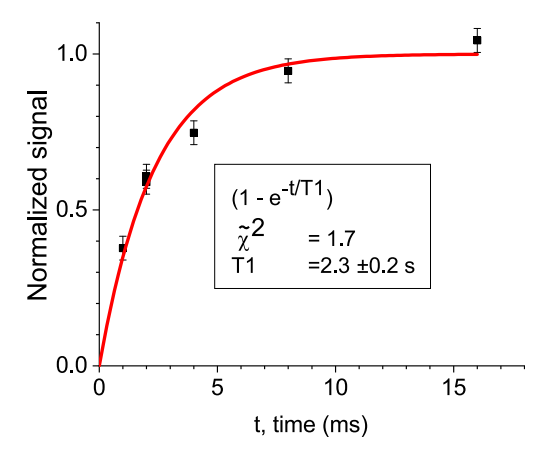


Fig. 5. Representative data taken at 26 °C. As the time between experiments increases, the signal returns to full value with a time constant of $T_1 = 2.3$ s.

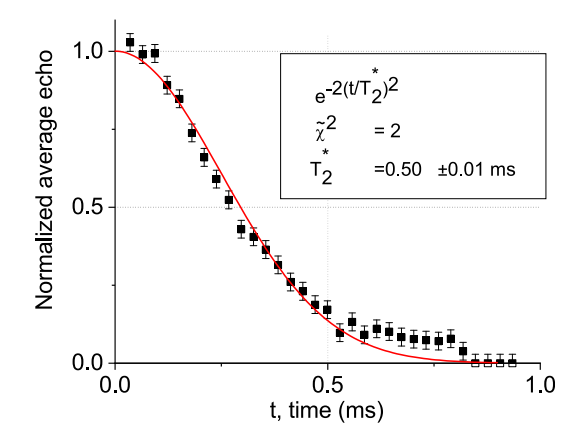


Fig. 6. The spin-echo, only half of which is shown due to dead time, decays to 14% in half a millisecond, or to 50% in 0.29 ms. The corresponding half-width-half-maximum is 0.75 kHz.

which was chosen based on indirect detection by double-resonance NQR/NMR experiments [15]. The spectrometer that was used was a Tecmag APOLLO [24]. The target sample of potassium has greater than 99% purity, with less than 0.001% heavy metal impurity.

4. Results

4.1. Resonance

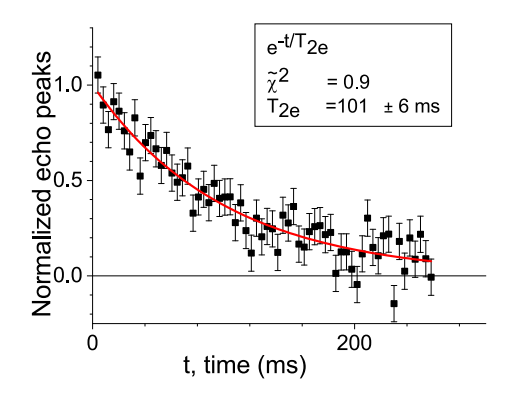
The NQR resonance frequency for potassium chlorate was found to have a linear dependence on temperature, over a limited temperature range near room temperature, as shown in Fig. 4. The temperature coefficient roughly agrees with earlier indirect-detection methods; Emshwiller [15] measured a frequency coefficient of \sim 1 kHz/°C for 41 K, or scaling for the quadrupole moments between isotopes, \sim 0.8 kHz for 39 K.

4.2. Relaxation rates

The spin-lattice relaxation time, shown in Fig. 5, determines how quickly the scans can be repeated. The value did not vary significantly over the temperature range studied, 17–31 °C, and the weighted average was $T_1 = 2.3 \pm 0.1$ s. The T_1 of ³⁹K in potassium nitrate is similar in value [17].

Within a single scan, spin echoes formed between refocusing pulses. The spin-echo was Gaussian in shape characterized by a time constant $T_2^* = 0.5$ ms, as shown in Fig. 6, a value shorter than the pulse-spacing at 2 ms. The pulse-spacing strongly effected the decay of the spin-echoes over the echo train as seen in Fig. 7. The decay time constant T_{2e} , decreases by a factor of four, as the pulse-spacing is increased by a factor of two, from 1 to 2 ms. Similar behavior has been previously observed during spin-3/2 NQR in other materials [26]. It is expected as the pulse-spacing of the refocusing pulse approaches T_2^* , T_{2e} will continue to increase.

In contrast to pulse-spacing, the refocusing pulse strength has only a weak effect on T_{2e} , as evidenced by the right graph in Fig. 8. The fast fourier transform (FFT) peak is maximized for a weaker pulse strength than the time domain amplitude. This shift, observed for 1 ms pulse-spacing, is caused by longer T_{2e} 's for weaker pulses. Lengthening of T_{2e} with weaker pulses has also been observed in 35 Cl in potassium chlorate [27]; in their work, however, the pulse spacing is significantly shorter than the spin-



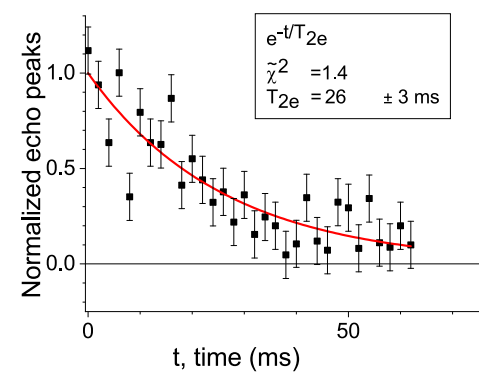


Fig. 7. The echo decay train produced by a refocusing pulse-spacing of 1 ms (Left), has a T_{2e} four times longer than the 2 ms spacing (Right).

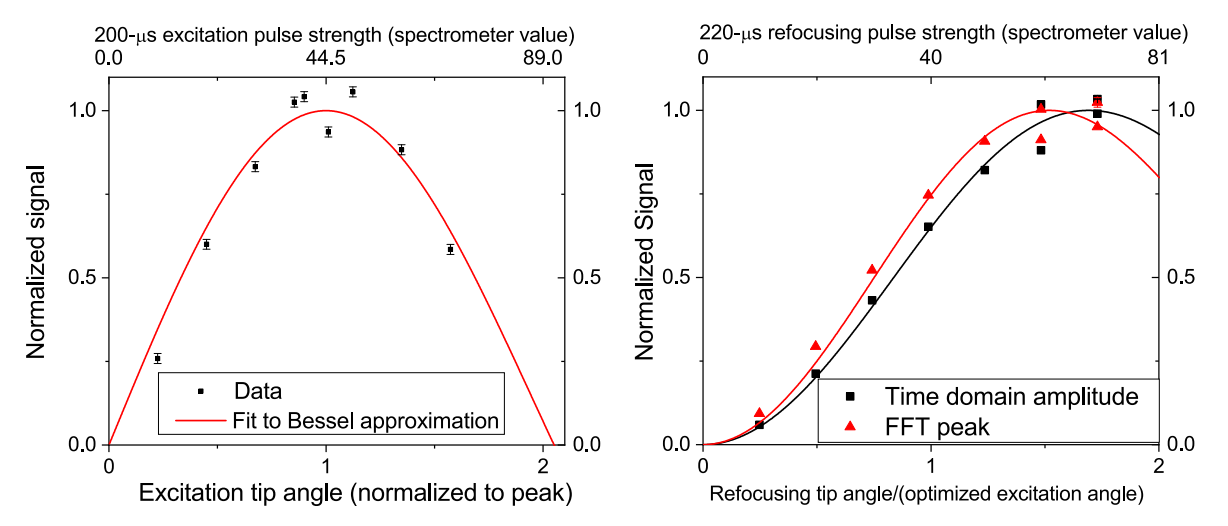


Fig. 8. Left: The excitation pulse is varied and the FFT of the echo train is fit to Eq. 10, with the refocusing pulse set to optimal. The variance seen in the graph reflects variations in the room temperature over the course of the experiment. Right: The refocusing pulse is varied, with the excitation pulse set to optimal. Both the FFT of the echo train (red), and the amplitude in the time-domain (black) is fit to Eq. 10. The net signal is optimized for weaker pulses than for the time-domain amplitudes, an indication T_{2e} is longer for weaker pulses.

spin relaxation and the lengthening more transparent. In addition, theoretical calculations for spin-3/2 NQR [28], indicate T_{2e} will depend on the strength of the pulse according to the type of linewidth broadening mechanism. This type of dependency has been observed in spin-1 systems[29,30]. With these observations, it is to be expected T_{2e} will become more sensitive to refocusing pulse strength for faster pulse-spacing, on par with T_2^* . Although we do see a weak dependence of T_{2e} on pulse strength, for a 1 ms pulse spacing, for 2 ms pulse spacing this dependence becomes negligible, underscoring the necessity for fast pulse-spacing.

5. Conclusion

In summary, 39 K in potassium chlorate was directly detected for the first time. Pulsed spin-locking was used to increase the duration of the signal, and the expected signal from N-echoes was derived. The prediction used many simplifying assumptions, chief of which is delta-function pulses which implicitly neglects any off-resonance effects during the pulse. Future work will refine the theory for finite pulses. Furthermore, key parameters important for detection were measured including, T_1, T_{2e}, T_2^* , as well as the temperature-dependent resonance frequency.

Ammonium nitrate can be used as a comparative baseline for detectability, as it possesses similar NQR frequencies to potassium chlorate. For a given volume, geometry, sensor, and measurement time, the $SNR \propto M \sqrt{\frac{T_{2e}}{f_1}}$, where M is the induced magnetization. The induced M for 39 K in potassium chlorate and for 14 N in ammonium nitrate are comparable. Taking into account Eq. 2 and Fig. 2, M from a potassium chlorate powder sample is $M = 0.36 \times 10^{-6} \frac{A}{m}$, while for ammonium nitrate $M = 0.30 \times 10^{-6} \frac{A}{m} [31]$. Therefore we focus on the metric $\sqrt{\frac{T_{2e}}{T_1}}$ in making comparisons.

Ammonium nitrate has two frequencies of interest, 497 kHz and 423 kHz. Due to variation in T_{2e} with pulse spacing, $\sqrt{\frac{T_{2e}}{T_1}}$ of both frequencies was 0.3 for a 4 ms pulse spacing [32], and increases to 0.4–0.5 for 2–3 ms spacing[33,34,32]. T_2^* is, in general, sample dependent [32], but was between 3 and 6 ms, on par with the pulse spacing, for the T_{2e} data discussed.

In contrast, 39 K in potassium chlorate, the metric $\sqrt{\frac{T_{2e}}{T_1}}=0.1$ for a 2 ms pulse-spacing. As the pulse-spacing decreases to 1 ms, the ideal SNR doubles. As pulse-spacing further decreases towards $T_2^*=0.5$ ms, T_{2e} along with the SNR should continue to significantly increase [29]. Therefore the detectability of potassium chlorate is poorer than ammonium nitrate for the longer pulse-spacing studied, but may very well approach that of ammonium nitrate for faster pulse-spacing.

Declaration of Competing Interest

The authors declare that they have no known competing financial interests or personal relationships that could have appeared to influence the work reported in this paper.

Acknowledgments

This work was supported by the National Science Foundation (award 1711118) as well as the US Army: Night Vision and Electronic Sensors Directorate. One of us (Nixon) was supported by the Office of Student Scholarship, Creative Activities, and Research (OSCAR) Undergraduate Research Scholars Program (URSP) at GMU.

Appendix A

A.1. Spin-locking due to isochromats in a single crystal

For an excitation pulse with frequency ω_0 , followed by N repetitions of (evolution time of duration τ , refocusing pulse, a second evolution time τ) the density matrix evolves as

$$\tilde{\rho}(t) = U^N U_0 \rho(0) U_0^{\dagger} U^{\dagger N}, \tag{11}$$

where U_0 is the unitary operator from the excitation pulse, and U is the unitary operator from the refocusing pulse and the evolution times. As indicated by the tilde, $\tilde{\rho}$, the density matrix description is done in the interaction representation of the dominant Hamiltonian

$$\hbar H_0 \equiv \frac{\omega_0}{\omega} \hbar H_Q, \tag{12}$$

where $\hbar H_0$ is the quadrupole Hamiltonian and ω is the spacing between levels [1],

$$\omega = \frac{3eQV_{zz}}{2I(2I-1)\hbar}\sqrt{1+\eta^2/3}.$$
 (13)

with Q as the quadrupole moment. The quadrupole Hamiltonian $\hbar H_0$ can be expressed as

$$H_{\mathbb{Q}} = \frac{1}{2}\omega z_1,\tag{14}$$

where the Pauli operators $[x_1, y_1, z_1]$ are given in Ref. [20].

The effective radio-frequency (RF) Hamiltonian, $\hbar H_{rf}$, taken in the delta-function limit, is

$$\hbar H_{rf} = \sqrt{3}\omega_1, \lambda x_1 z_2' \cos(\omega_0 t + \varphi), \tag{15}$$

where z_2' corresponds to a second set of Pauli operators [20] that commute with the first set, $\omega_1 = \gamma B_1/2$ and λ is given by Eq. 4. Under the secular approximation, the RF Hamiltonian depends on the phase φ of the pulse by:

$$\widetilde{H}_{rf}(\varphi=0) = \frac{\sqrt{3}}{2}\omega_1 \lambda x_1 z_2', \tag{16}$$

$$\widetilde{H}_{rf}(\varphi = \pi/2) = \frac{\sqrt{3}}{2}\omega_1 \lambda y_1 z_2'. \tag{17}$$

During the evolution time the Hamiltonian is $\hbar H_e$

$$H_e = \frac{\delta}{2} z_1,\tag{18}$$

where $\delta = \omega_0 - \omega$. Therefore

$$U_0 = e^{-i\theta_0 x_1 z_2'}, \ U = e^{-i\theta_a z_1} e^{-i\theta_b y_1 z_2'} e^{-i\theta_a z_1}, \tag{19}$$

$$\theta_0 = \lambda \frac{\sqrt{3}}{3} \omega_1 t_p = \lambda \frac{\Theta}{3},\tag{20}$$

$$\theta_0 = \lambda \frac{\sqrt{3}}{2} \omega_1 t_p = \lambda \frac{\Theta}{2}, \tag{20}$$

$$\theta_a = \frac{\delta \tau}{2}, \tag{21}$$

$$\theta_b = \frac{\sqrt{3}}{2} \omega_1 \lambda t_p' = \lambda \Theta', \tag{22}$$

where t_p is the duration of the excitation pulse with $\varphi = 0$ and t'_p is the duration of the refocusing pulse with $\varphi = \pi/2$. The rotation *U* simplifies to [35,36]

$$U = e^{-i\theta_{ab}\boldsymbol{\sigma}\cdot\hat{n}_{ab}} \text{ and } (23)$$

 $U^N=e^{-iN heta_{ab}m{\sigma}\cdot\hat{n}_{ab}}$, where the Pauli - like operator vector

$$\boldsymbol{\sigma} = x_1 z_2' \hat{x}_1 + y_1 z_2' \hat{y}_1 + z_1 \hat{z}_1, \tag{25}$$

$$\cos \theta_{ab} = \cos 2\theta_a \cos \theta_b$$
 and (26)

$$\sin \theta_{ab} \hat{n}_{ab} = \sin \theta_b \hat{y}_1 + \sin 2\theta_a \cos \theta_b \hat{z}_1. \tag{27}$$

At t = 0, the system is in thermal equilibrium and the effective

$$\rho(0) = \frac{\omega \hbar}{8kT} z_1. \tag{28}$$

After the excitation pulse the density matrix is:

$$\frac{\omega\hbar}{8kT} \left[z_1 \cos 2\theta_0 - y_1 z_2' \sin 2\theta_0 \right]. \tag{29}$$

After N refocusing pulses, and taking into account phase cycling (θ_0 changes sign and the signals are subtracted), the density matrix becomes

$$\tilde{\rho}(t) = \frac{\omega h \sin 2\theta_0}{8kT}
\left[-\hat{y}_1 \cdot \boldsymbol{\sigma} \cos 2N\theta_{ab} + 2(\hat{n}_{ab} \cdot \hat{y}_1)\hat{n}_{ab} \cdot \boldsymbol{\sigma} \sin^2 N\theta_{ab} \right. (30)
+ (\hat{y}_1 \times \hat{n}_{ab}) \cdot \boldsymbol{\sigma} \sin 2N\theta_{ab} \right].$$

Considering equal and opposite off-resonant isochromats, the final term will average out, leaving

$$\tilde{\rho}(t) = \frac{-\omega\hbar\sin 2\theta_0}{8kT} y_1 z_2' \left[1 - 2\sin^2 N\theta_{ab} (\hat{n}_{ab} \cdot \hat{z}_1)^2 \right]. \tag{31}$$

For detection by the same coil, it is necessary to find the magnetic moment along \widehat{X} ,

$$\mu_{X} = \gamma \hbar \left\langle \tilde{I}_{X} \tilde{\rho}(t) \right\rangle \tag{32}$$

$$= \lambda \left(Tr\{x_1 z_2' \tilde{\rho}(t)\} \cos \omega_0 t - Tr\{y_1 z_2' \tilde{\rho}(t)\} \sin \omega_0 t \right). \tag{33}$$

Using Eq. 30 and Eq. 31,

$$\mu_{X} = \frac{\gamma \hbar^{2} \omega \sqrt{3}}{4kT} \lambda \sin 2\theta_{0} \left[1 - 2 \sin^{2} N\theta_{ab} (\hat{n}_{ab} \cdot \hat{z}_{1})^{2} \right] \sin \omega_{0} t. \tag{34}$$

After only one refocusing pulse, the amplitude of the magnetic moment reduces to

$$\mu_{X}(N=1) = \frac{\gamma \hbar^{2} \omega \sqrt{3}}{4kT} \lambda \sin \lambda \Theta \left[\sin^{2} \lambda \Theta' + \cos(4\delta \tau) \cos^{2} \lambda \Theta' \right]. \quad (35)$$

The first term has no dependence on off-resonance and is the echo, the second term will average to zero for a large enough linewidth, as is the case for potassium chlorate.

The average over N echoes [37] is

$$\bar{\mu}_{X} = \frac{\gamma \hbar \omega \sqrt{3}}{4kT} \lambda \sin 2\theta_{0}$$

$$\left[(\hat{n}_{ab} \cdot \hat{y}_{1})^{2} + \frac{\cos(N+1)\theta_{ab}\sin N\theta_{ab}}{N\sin\theta_{ab}} (\hat{n}_{ab} \cdot \hat{z}_{1})^{2} \right] \sin\omega_{0}t.$$
(36)

In the limit of a large number of echoes, the second term goes to zero. Therefore the spin-locked terms comes down to the evaluation from Eq. 31,

$$\left(\hat{n}_{ab} \cdot \hat{y}_1\right)^2 = \frac{\sin^2 \theta_b}{\sin^2 \theta_b + \cos^2 \theta_b \sin^2 2\theta_a}.$$
 (37)

The spins are fully locked, $(\hat{n}_{ab} \cdot \hat{y}_1)^2 = 1$, in the limit where $\theta_b = \pi/2$ regardless of off-resonance, or in the trivial limit with no off-resonance, $\theta_a = 0$. The former condition can not be met in a powder sample. We can, however, put a minimum limit on the spin-locking, corresponding to the condition $\sin^2 2\theta_a = 1$. Therefore the amplitude of the minimum locked signal, without taking into account other sources of decoherence, would be:

$$\bar{\mu}_{X-min} = \frac{\gamma \hbar^2 \omega \sqrt{3}}{4kT} \lambda \sin \lambda \Theta \sin^2 \lambda \Theta'. \tag{38}$$

This expression is identical to the echo after the first refocusing pulse.

A.2. Signal-to-noise ratio

The time constant T_{2e} determines the optimal number of echoes. Assuming a single-exponential time constant, in the limit of delta-function pulses and no instrumental dead time, the average signal over the echoes acquired over a time t is

$$\overline{S} = \frac{S_0}{t} \int_0^t e^{-\frac{t'}{T_{2e}}} dt' = S_0 \frac{T_{2e}}{t} \left[1 - e^{-\frac{t}{T_{2e}}} \right], \tag{39}$$

where S_0 is the initial amplitude of the signal. The noise, n, is $s\sqrt{1/t}$, where s is the sensitivity of the sensor. Therefore, the signal-tonoise ratio for one echo train is

$$SNR_1 = \frac{S_0}{s} \sqrt{T_{2e}} \frac{[1 - e^{-x}]}{\sqrt{x}}, \tag{40} \label{eq:40}$$

where $x = \frac{t}{T_{10}}$. The optimal value of x is 1.25.

The time constant T_1 determines t_d , the spacing between experiments. The relationship between T_1 and t_d is shown by

$$S_0 = S_{\infty} \left[1 - e^{-\frac{t_d}{I_1}}, \right], \tag{41}$$

where S_{∞} is the signal with infinite time between scans. The value for S_{∞} depends on the number density of the targeted nuclei and the induced magnetic moment. The SNR increases with repeated measurements. Assuming x = 1.25, with repeated scans = $\frac{T_{tot}}{1.25T_{ro} + t_{e'}}$

$$SNR = \frac{S_{\infty}}{2s} \left\{ 2 \frac{\left[1 - e^{-1.25}\right]}{\sqrt{1.25}} \frac{\left[1 - e^{-y}\right]}{\sqrt{y + 1.25b}} \right\} \sqrt{\frac{T_{2e}}{T_1}} \sqrt{T_{tot}}, \tag{42} \label{eq:42}$$

where $y = \frac{t_d}{T_1}$ and $b = \frac{T_{2e}}{T_1}$. Letting

$$\alpha = 2 \frac{\left[1 - e^{-1.25}\right]}{\sqrt{1.25}} \frac{\left[1 - e^{-y}\right]}{\sqrt{y + 1.25b}},\tag{43}$$

$$SNR = \alpha \left\{ \frac{S_{\infty}}{2s} \sqrt{\frac{T_{2e}}{T_1}} \right\} \sqrt{T_{tot}}. \tag{44}$$

Note, for 0 < b < 1, the optimal α occurs over the range of 1.25 < y < 2 and has a value of $0.71 < \alpha < 0.95$.

References

- [1] B.H. Suits, Nuclear quadrupole resonance spectroscopy, in: D.R. Vij (Ed.), Handbook of Applied Solid State Spectroscopy, Springer US, Boston, MA, 2006,
- A. Ohte, H. Iwaoka, K. Mitsui, H. Sakurai, A. Inaba, Accurate Calibration of a New NQR Thermometer (203 K to 398 K Range Calibration at the NRLM), Metrologia 15 (1979) 195-199.
- M. Huebner, J. Leib, G. Eska, NOR on Gallium Single Crystals for Absolute Thermometry at Very Low Temperatures, J. Low Temp. Phys. 114 (1999) 203-
- [4] A. Samila, I. Safronov, O. Hotra, Structural and functional synthesis of the continuous wave NOR temperature sensor with increased conversion linearity, Solid State Nucl. Magn. Reson. 110 (2020) 101700.
- [5] J. Lužnik, J. Pirnat, Z. Trontelj, Measurement of temperature and temperature gradient in millimeter samples by chlorine NQR, Appl. Phys. A 96 (2009) 1023-
- [6] V. Khandozhko, N. Raranskii, V. Balazjuk, A. Samila, Z. Kovalyuk, Temperature and baric dependence of nuclear quadruple resonance spectra in indium and gallium monoselenides, in: O.V. Angelsky (Ed.), Eleventh International Conference on Correlation Optics, vol. 9066, International Society for Optics and Photonics, SPIE, 2013, pp. 423-429.
- A.J. Vega, ⁶³Cu NQR Nutation Spectroscopy and Spin Counting in Copper Oxides, Isr. J. Chem. 32 (2-3) (1992) 195-204.
- M. Moroni, P. Carretta, G. Allodi, R. De Renzi, M.N. Gastiasoro, B.M. Andersen, P. Materne, H.-H. Klauss, Y. Kobayashi, M. Sato, S. Sanna, Fast recovery of the stripe magnetic order by Mn/Fe substitution in F-doped LaFeAsO superconductors, Phys. Rev. B 95 (2017) 180501.
- P. Carretta, G. Prando, Iron-based superconductors: tales from the nuclei, Riv. Nuovo Cim 43 (1) (2020) 133-141.
- [10] T.M. Osán, L.M. Cerioni, J. Forguez, J.M. Ollé, D.J. Pusiol, NQR: From imaging to explosives and drugs detection, Phys. B: Condens. Matter 389 (1) (2007) 45-50, Proceedings of the International Workshop 35th Anniversary of Hyperfine Interactions at La Plata and Humboldt Kolleg on Solid State Physics.
- [11] J.B. Miller, G.A. Barrall, Explosives Detection with Nuclear Quadrupole Resonance: An emerging technology will help to uncover land mines and terrorist bombs, Am. Sci. 93 (1) (2005) 50-57.

- [12] A. Garroway, M. Buess, J. Miller, B. Suits, A. Hibbs, G. Barrall, R. Matthews, L. Burnett, Remote sensing by nuclear quadrupole resonance, IEEE Trans. Geosci. Remote Sens. 39 (6) (2001) 1108-1118.
- T. Kushida, G.B. Benedek, N. Bloembergen, Dependence of the Pure Quadrupole Resonance Frequency on Pressure and Temperature, Phys. Rev. 104 (1956) 1364-1377
- S.-K. Lee, K.L. Sauer, S.J. Seltzer, O. Alem, M.V. Romalis, Subfemtotesla radiofrequency atomic magnetometer for detection of nuclear quadrupole resonance, Appl. Phys. Lett. 89 (21) (2006) 214106.
- [15] M. Emshwiller, E.L. Hahn, D. Kaplan, Pulsed Nuclear Resonance Spectroscopy, Phys. Rev. 118 (1960) 414-424.
- [16] R.S. Cantor, J. Waugh, Pulsed spin locking in pure nuclear quadrupole resonance, J. Chem. Phys. 73 (1980) 1054.
- [17] J.B. Miller, Nuclear quadrupole resonance detection of explosives, in: J. Yinon (Ed.), Counterterrorist Detection Techniques of Explosives, Elsevier Science B. V., Amsterdam, 2007, pp. 157-198 (Chapter 7).
- [18] C. Odin, Calculations of Multipulse Sequence in NQR of Spins 3/2, J. Magn. Reson. 141 (2) (1999) 239-255.
- [19] C. Odin, Repetitive experiments of one or two-pulse sequences in NQR of spins I=3/2: Liouville space, steady-state, Ernst angle and optimum signal, Solid State Nucl. Magn. Reson. 85 (2017) 25-33.
- [20] M. Goldman, "Spin-1/2 Description of Spins," in Advances in Magnetic Resonance, in: W.S. Warren (Ed.), Advances in Magnetic and Optical Resonance, vol. 14, Academic Press, 1990, pp. 59-74.
- [21] Y. Xia, C. Ye, NQR spectroscopy of powder sample with spin I=1 and 3/2 responses to pulses, Prog. Nat. Sci. Mater. Int. 6 (1996) 290-292.
- [22] Y. Xia, Y. Shi, C. Ye, NQR spectroscopy of powder sample with spin I=1 and 3/2 (ii) - responses to pulses, Prog. Nat. Sci. 6 (4) (1996) 420–421.
 [23] T.J. Bastow, Powder determination of ³⁹K nuclear quadrupole coupling, J.
- Chem. Soc., Faraday Trans. 87 (1991) 2453–2455.
- [24] Tecmag, "Apollo".
- [25] S. Industries, SP Scientific Air Jet Sample Cooler System Model XRII851.
- N.E. Ainbinder, G.B. Furman, G.E. Kibrik, A.Y. Poljakov, I.G. Shaposhnikov, Relaxation Processes in NQR Multiple-Pulse Spin-Locking, Zeitschrift für Naturforschung A 41 (1-2) (1986) 366-369.
- [27] N. Reddy, P. Narasimhan, Multiple-pulse investigations in pure NQR spectroscopy: influence of spin-locking and phase alternated pulse sequence (PAPS) on polycrystalline samples containing ³⁵Cl(I= 3/2) nuclei, J. Mol. Struct. 192(3) (1989) 345-354. Proceedings of the 9th International Symposium on Nuclear Quadrupole Resonance.
- [28] A. Dubey, P. Narasimhan, Multiple pulse response in pure NQR of spin I = 3/2 nuclei in single crystals: response to phase-alternated pulse sequence (PAPS), J. Mol. Struct. 192(3) (1989) 321-331. Proceedings of the 9th International Symposium on Nuclear Quadrupole Resonance.
- [29] M.W. Malone, M. McGillvray, K.L. Sauer, Revealing dipolar coupling with NQR off-resonant pulsed spin locking, Phys. Rev. B 84 (2011) 214430.
- [30] M. Malone, K. Sauer, Heteronuclear dipolar coupling in spin-1 NQR pulsed spin locking, J. Magn. Reson. 238 (2014) 8-15.
- [31] S. Vega, Theory of T₁ relaxation measurements in pure nuclear quadrupole resonance for spins I = 1, J. Chem. Phys. 61 (3) (1974) 1093–1100.
- [32] J. Barras, M. Gaskell, N. Hunt, et al., Detection of Ammonium Nitrate inside Vehicles by Nuclear Quadrupole Resonance, Appl. Magn. Reson. 25 (2004)
- [33] D. Prescott, Nuclear Quadrupole Spin Dynamics: How Weak RF Pulses and Double Resonance Cross-Relaxation Contribute to Explosives Detection, PhD thesis, University of George Mason, 2010.
- L. Cardona, Y. Miyato, H. Itozaki, et al., Remote Detection of Ammonium Nitrate by Nuclear Quadrupole Resonance using a Portable System, Appl. Magn. Reson. 46 (2015) 295-307.
- C. Counsell, M. Levitt, R. Ernst, Analytical theory of composite pulses, J. Magn. Reson. (1969) 63 (1) (1985) 133-141.
- [36] K.L. Sauer, C.A. Klug, J.B. Miller, A.N. Garroway, Using quaternions to design composite pulses for spin-1 NQR, Appl. Magn. Reson. 25 (2004) 485.
- [37] I.S. Gradshteyn, I.M. Ryzhik, Table of integrals, series, and products, seventh ed., Elsevier/Academic Press, Amsterdam, 2007. Translated from the Russian, Translation edited and with a preface by Alan Jeffrey and Daniel Zwillinger, With one CD-ROM (Windows, Macintosh and UNIX).